On-chip visible-to-infrared supercontinuum generation with more than 495 THz spectral bandwidth

Jörn P. Epping,[1,*] Tim Hellwig,[2] Marcel Hoekman,[3] Richard Mateman,[3] Arne Leinse,[3] René G. Heideman,[3] Albert van Rees,[4] Peter J.M. van der Slot,[1] Chris J. Lee,[1] Carsten Fallnich,[1,2] and Klaus-J. Boller[1]

[1]*MESA+ Institute for Nanotechnology, University of Twente, Enschede 7500 AE, The Netherlands*

[2]*Institute of Applied Physics, Westfälische Wilhelms-Universität, Corrensstrasse 2, 48149 Münster, Germany*

[3]*LioniX B.V., PO Box 456, Enschede 7500 AL, The Netherlands*

[4]*XiO Photonics B.V., PO Box 1254, Enschede 7500 BG, The Netherlands*

[*]*j.p.epping@utwente.nl*

Abstract: We report ultra-broadband supercontinuum generation in high-confinement Si_3N_4 integrated optical waveguides. The spectrum extends through the visible (from 470 nm) to the infrared spectral range (2130 nm) comprising a spectral bandwidth wider than 495 THz, which is the widest supercontinuum spectrum generated on a chip.

OCIS codes: (130.0130) Integrated optics; (190.7110) Ultrafast nonlinear optics; (320.6629) Supercontinuum generation.

References and links

1. G. Humbert, W. Wadsworth, S. Leon-Saval, J. Knight, T. Birks, P. S. J. Russell, M. Lederer, D. Kopf, K. Wiesauer, E. Breuer, and D. Stifter, "Supercontinuum generation system for optical coherence tomography based on tapered photonic crystal fibre," Opt. Express **14**(4), 1596 (2006).
2. L. Yin, Q. Lin, and G. P. Agrawal, "Soliton fission and supercontinuum generation in silicon waveguides," Opt. Lett. **32**(4), 391 (2007).
3. M. Wulf, D. M. Beggs, N. Rotenberg, and L. Kuipers, "Unravelling nonlinear spectral evolution using nanoscale photonic near-field point-to-point measurements," Nano Lett. **13**(12), 5858–5865 (2013).
4. J. M. Dudley, G. Genty, and B. J. Eggleton, "Harnessing and control of optical rogue waves in supercontinuum generation," Opt. Express **16**(6), 3644 (2008).
5. H. Kano and H.-O. Hamaguchi, "Characterization of a supercontinuum generated from a photonic crystal fiber and its application to coherent Raman spectroscopy," Opt. Lett. **28**(23), 2360 (2003).
6. J. T. Woodward, A. W. Smith, C. A. Jenkins, C. Lin, S. W. Brown, and K. R. Lykke, "Supercontinuum sources for metrology," Metrologia **46**(4), S277 (2009).
7. F. Silva, D. Austin, A. Thai, M. Baudisch, M. Hemmer, D. Faccio, A. Couairon, and J. Biegert, "Multi-octave supercontinuum generation from mid-infrared filamentation in a bulk crystal," Nat. Commun. **3**, 807 (2012).
8. T. A. Birks, W. J. Wadsworth, and P. S. J. Russell, "Supercontinuum generation in tapered fibers," Opt. Lett. **25**(19), 1415 (2000).
9. A. Marandi, C. W. Rudy, V. G. Plotnichenko, E. M. Dianov, K. L. Vodopyanov, and R. L. Byer, "Mid-infrared supercontinuum generation in tapered chalcogenide fiber for producing octave-spanning frequency comb around 3 μm," Opt. Express **20**(22), 24218–24225 (2012).
10. J. M. Dudley and S. Coen, "Supercontinuum generation in photonic crystal fiber," Rev. Mod. Phys. **78**(4), 1135–1184 (2006).
11. M. Klimczak, G. Stepniewski, H. Bookey, A. Szolno, R. Stepien, D. Pysz, A. Kar, A. Waddie, M. R. Taghizadeh, and R. Buczynski, "Broadband infrared supercontinuum generation in hexagonal-lattice tellurite photonic crystal fiber with dispersion optimized for pumping near 1560 nm," Opt. Lett. **38**(22), 4679–4682 (2013).

#241128 Received 18 May 2015; revised 25 Jun 2015; accepted 26 Jun 2015; published 20 Jul 2015

12. X. Jiang, N. Y. Joly, M. A. Finger, F. Babic, G. K. L. Wong, J. C. Travers, and P. S. J. Russell, "Deep-ultraviolet to mid-infrared supercontinuum generated in solid-core ZBLAN photonic crystal fibre," Nat. Photonics **9**(2), 133–139 (2015).
13. C. R. Phillips, C. Langrock, J. S. Pelc, M. M. Fejer, J. Jiang, M. E. Fermann, and I. Hartl, "Supercontinuum generation in quasi-phase-matched $LiNbO_3$ waveguide pumped by a Tm-doped fiber laser system," Opt. Lett. **36**(19), 3912–3914 (2011).
14. B. Rangarajan, A. Y. Kovalgin, K. Wörhoff, and J. Schmitz, "Low-temperature deposition of high-quality silicon oxynitride films for CMOS-integrated optics," Opt. Lett. **38**(6), 941–943 (2013).
15. F. Leo, S.-P. Gorza, J. Safioui, P. Kockaert, S. Coen, U. Dave, B. Kuyken, and G. Roelkens, "Dispersive wave emission and supercontinuum generation in a silicon wire waveguide pumped around the 1550 nm telecommunication wavelength," Opt. Lett. **39**(12), 3623–3626 (2014).
16. B. Kuyken, T. Ideguchi, S. Holzner, M. Yan, T. W. Hänsch, J. Van Campenhout, P. Verheyen, S. Coen, F. Leo, R. Baets, G. Roelkens, and N. Picqué, "An octave-spanning mid-infrared frequency comb generated in a silicon nanophotonic wire waveguide," Nat. Commun. **6**, 6310 (2015).
17. D. Y. Oh, D. Sell, H. Lee, K. Y. Yang, S. A. Diddams, and K. J. Vahala, "Supercontinuum generation in an on-chip silica waveguide," Opt. Lett. **39**(4), 1046–1048 (2014).
18. D. Duchesne, M. Peccianti, M. R. E. Lamont, M. Ferrera, L. Razzari, F. Légaré, R. Morandotti, S. Chu, B. E. Little, and D. J. Moss, "Supercontinuum generation in a high index doped silica glass spiral waveguide," Opt. Express **18**(2), 923–930 (2010).
19. R. Halir, Y. Okawachi, J. S. Levy, M. A. Foster, M. Lipson, and A. L. Gaeta, "Ultrabroadband supercontinuum generation in a CMOS-compatible platform," Opt. Lett. **37**(10), 1685–1687 (2012).
20. J. M. Chavez Boggio, D. Bodenmüller, T. Fremberg, R. Haynes, M. M. Roth, R. Eisermann, M. Lisker, L. Zimmermann, and M. Böhm, "Dispersion engineered silicon nitride waveguides by geometrical and refractive-index optimization," J. Opt. Soc. Am. B **31**(11), 2846 (2014).
21. H. Zhao, B. Kuyken, S. Clemmen, F. Leo, A. Subramanian, A. Dhakal, P. Helin, S. Severi, E. Brainis, G. Roelkens, and R. Baets, "Visible-to-near-infrared octave spanning supercontinuum generation in a silicon nitride waveguide," Opt. Lett. **40**(10), 2177–2180 (2015).
22. A. Gondarenko, J. S. Levy, and M. Lipson, "High confinement micron-scale silicon nitride high Q ring resonator," Opt. Express **17**(14), 11366–11370 (2009).
23. J. F. Bauters, M. J. R. Heck, D. John, D. Dai, M.-c. Tien, J. S. Barton, A. Leinse, R. G. Heideman, D. J. Blumenthal, and J. E. Bowers, "Ultra-low-loss high-aspect-ratio Si_3N_4 waveguides," Opt. Express **19**(4), 3163–3174 (2011).
24. K. Ikeda, R. E. Saperstein, N. Alic, and Y. Fainman, "Thermal and Kerr nonlinear properties of plasma-deposited silicon nitride/silicon dioxide waveguides," Opt. Express **16**(17), 12987–12994 (2008).
25. C. G. H. Roeloffzen, L. Zhuang, C. Taddei, A. Leinse, R. G. Heideman, P. W. L. van Dijk, R. M. Oldenbeuving, D. A. I. Marpaung, M. Burla, and K.-J. Boller, "Silicon nitride microwave photonic circuits," Opt. Express **21**(19), 22937–22961 (2013).
26. E. S. Hosseini, P. Purnawirman, J. D. B. Bradley, J. Sun, G. Leake, T. N. Adam, D. D. Coolbaugh, and M. R. Watts, "CMOS-compatible 75 mW erbium-doped distributed feedback laser," Opt. Lett. **39**(11), 3106–3109 (2014).
27. L. Zhang, Y. Yan, Y. Yue, Q. Lin, O. Painter, R. G. Beausoleil, and A. E. Willner, "On-chip two-octave supercontinuum generation by enhancing self-steepening of optical pulses," Opt. Express **19**(12), 11584–11590 (2011).
28. J. Riemensberger, K. Hartinger, T. Herr, V. Brasch, R. Holzwarth, and T. J. Kippenberg, "Dispersion engineering of thick high-Q silicon nitride ring-resonators via atomic layer deposition," Opt. Express **20**(25), 27661–27669 (2012).
29. J. P. Epping, M. Hoekman, R. Mateman, A. Leinse, R. G. Heideman, A. van Rees, P. J. van der Slot, C. J. Lee, and K.-J. Boller, "High confinement, high yield Si_3N_4 waveguides for nonlinear optical applications," Opt. Express **23**(2), 642 (2015).
30. K. Wörhoff, R. G. Heideman, A. Leinse, and M. Hoekman, "TriPleX: a versatile dielectric photonic platform," Adv. Opt. Techn. **4**(2), 189–207 (2015).
31. A. B. Fallahkhair, K. S. Li, and T. E. Murphy, "Vector finite difference modesolver for anisotropic dielectric waveguides," J. Lightwave Technol. **26**(11), 1423–1431 (2008).
32. F. Poletti and P. Horak, "Description of ultrashort pulse propagation in multimode optical fibers," J. Opt. Soc. Am. B **25**(10), 1645–1654 (2008).
33. G.P. Agrawal, *Nonlinear Fiber Optics*, 4th ed. (Academic Press, 2007).
34. D. J. Jones, S. A. Diddams, J. K. Ranka, A. Stentz, R. S. Windeler, J. L. Hall, and S. T. Cundiff, "Carrier-envelope phase control of femtosecond mode-locked lasers and direct optical frequency synthesis," Science **288**(5466), 635–639 (2000).
35. J. P. Epping, M. Kues, P. J. M. van der Slot, C. J. Lee, C. Fallnich, and K.-J. Boller, "Integrated CARS source based on seeded four-wave mixing in silicon nitride," Opt. Express **21**(26), 32123–32129 (2013).

#241128 Received 18 May 2015; revised 25 Jun 2015; accepted 26 Jun 2015; published 20 Jul 2015

1. Introduction

Ultra-broadband optical spectra obtained by supercontinuum generation (SCG) have found wide-spread use in applications and fundamental research. Examples are optical coherence tomography [1], unraveling nonlinear dynamics [2–4], coherent spectroscopy [5], and frequency metrology [6]. Of particular interest is extending SCG into the visible range and beyond, which has so far been possible only with bulk nonlinear media [7], tapered fibers [8, 9], photonic crystal fibers [10–12], and $\chi^{(2)}$ nonlinear waveguides [13].

A major disadvantage of these approaches is their lack of CMOS compatibility, because CMOS compatibility allows for fabrication of devices in high volumes using established facilities and for photonic integration with electronic circuits [14]. A well-known CMOS-compatible waveguide platform is provided in silicon photonics, where a large nonlinear coefficient ($\gamma \approx 300$ W^{-1}m^{-1}) is available to overcome waveguide losses and provide highly efficient SCG [15, 16]. However, the small band gap of silicon, corresponding to about 1 μm wavelength, limits the wavelength range of supercontinua to the infrared. Another limit is that at the high intensities needed for ultra-broadband SCG, pump wavelengths shorter than 2 μm, such as in the 1.3 and 1.5 μm telecommunication bands, suffer from nonlinear losses occurring in silicon such as two-photon absorption and subsequent free-carrier absorption.

A most promising CMOS-compatible approach for extending on-chip SCG into the visible range is based on silica [17, 18] and silicon nitride [19–21] glass platforms, which offer excellent transparency down to the ultraviolet. Specifically, low-pressure chemical vapor deposition (LPCVD) of stoichiometric materials [22] offers highly reproducible fabrication with predefined material dispersion and extremely low-loss waveguides (¡ 0.1 dB/m) [23]. For optimally exploiting the Kerr index of Si_3N_4, $n_2 = 2.4 \cdot 10^{-19}$ m^2/W [24], the optical mode can be tightly confined due to the high-contrast offered by the silicon nitride based glass platform, thereby offering an increased nonlinear coefficient ($\gamma \approx 1$ W^{-1}m^{-1}). Additional advantages are the options available for integrating extended waveguide circuitries [25], as well as rare-earth-doped lasers [26].

The widest supercontinuum spectra obtained in CMOS-compatible platforms to date were generated with silicon nitride waveguides, using ultrashort pulses at 1.5 μm wavelength in a 1.4 cm long waveguide [20] and at 1.3 μm wavelength in a 4.3 cm long waveguide [19]. The latter yielded some output at the edge of the visible range (¿ 665 nm). Improved engineering of the dispersion was proposed [27] and applied for further spectral broadening [20, 28], however, for SCG, the output remained at wavelengths longer than 700 nm. Most recent experiments successfully extended the SCG towards the blue range [21] with a spectral bandwidth of 310 THz in a 1 cm long underetched waveguide. These results show that, to obtain shorter wavelength supercontinua on a chip, a shorter wavelength pump is required and, consequently, suitable dispersion for a shorter pump wavelength has to be provided.

Here, we report ultra-broadband supercontinuum generation in high-confinement stoichiometric Si_3N_4 integrated optical waveguides. The SCG extends from the blue wavelength range (470 nm) to the infrared spectral range (2130 nm). This range comprises a spectral bandwidth of more than 495 THz which is, to our knowledge, the widest supercontinuum ever generated on a chip. The generation of such a wide spectral bandwidth supercontinuum is made possible by our novel technique for reliable fabrication of high thickness (up to $\sim$1 μm), crack-free waveguides using LPCVD [29, 30]. The increased waveguide dimensions are used to shift the zero dispersion wavelength (ZDW) to values as short as 1 μm for phase-matched excitation with a mode-locked 1064 nm Yb-fiber laser, thereby extending the short-wavelength edge of the supercontinuum and obtain ultra-broadband SCG at a propagation length as short as 5.5 mm.

#241128 Received 18 May 2015; revised 25 Jun 2015; accepted 26 Jun 2015; published 20 Jul 2015

2. Dispersion calculation

The scanning electron microscope (SEM) picture in Fig. 1(a) shows a typical example of the cross section of the waveguides used in this experiment with a Si_3N_4 waveguide core shown in red and a SiO_2 cladding shown in blue. It can be seen that the lower part of the cross section has a rounded shape. For calculating the waveguide dispersion, this shape was taken into account in the form of step index profiles as found in the SEM images. The optical modes and their effective refractive indices were calculated using a finite element solver [31] for a wavelength range from 400 to 2500 nm. The calculated dispersion parameter, D, for the fundamental quasi-TM modes and waveguides with a height, h, of 1.0 μm and widths, w, of 0.70, 0.75, and 0.80 μm, respectively, is shown in Fig. 1(b). These particular dimensions were chosen so that light with a pump wavelength of 1064 nm, such as conveniently available from Yb- or Nd-doped lasers, experiences anomalous dispersion ($D > 0$), which is not the case for bulk Si_3N_4 (red dashed line). We note that increasing the waveguide width (from 0.70 μm to 0.80 μm) increases the wavelength range that experiences anomalous dispersion by 170 nm. This means that a broader bandwidth is expected from wider waveguides. Another result of the increased waveguide dimensions is that the waveguide supports three modes at the pump wavelength in the TM polarization, namely the fundamental TM_{00} and two higher order modes TM_{10} and TM_{20}.

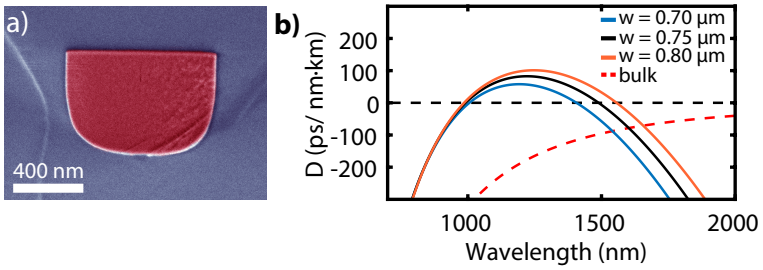

Fig. 1. (a) SEM picture (false color) of a waveguide facet. (b) Calculated dispersion parameter, D, for bulk Si_3N_4 (red dashed line) and Si_3N_4 waveguides with $h = 1.0$ μm and various waveguide widths, w, of 0.70 μm (blue), 0.75 μm (black), and 0.80 μm (orange) for fundamental quasi-TM modes. The calculations take into account the rounded shape of the waveguides [29]. As can be seen, the range of anomalous dispersion ($D > 0$) increases with the waveguide width, allowing the two zero dispersion wavelengths (ZDW) to be tuned from 1010 nm and 1410 nm at $w = 0.70$ μm to 990 nm and 1560 nm at $w = 0.80$ μm.

3. Experimental results

The experimental setup for SCG is depicted in Fig. 2. Ultrashort pulses with a center wavelength of 1064 nm are provided with a mode-locked Yb-doped fiber laser (Ekspla, LightWire FF200). The laser provides pulses with about 115 fs duration, a repetition rate of 41 MHz, and a maximum average output power of 200 mW (maximum pulse energy 5 nJ). The pulses are coupled into the Si_3N_4 waveguides with a coupling loss of about 9 dB using an aspheric lens. The two particular chips selected here, out of 40 chips, contain 20 waveguides of various widths each with a height of 1.0 μm, and a length of 5.5 mm. To control the pump power, a half-wave plate and a polarizing beam splitter are used. A second half-wave plate is used to set the input polarization for excitation of quasi-TM modes. The supercontinuum is collected using a lensed fiber and recorded using an optical spectrum analyzer (Ando AQ6315A) and a near-infrared spectrometer (Avantes NIRline). To minimize the collection of undesired scattered light during

#241128 Received 18 May 2015; revised 25 Jun 2015; accepted 26 Jun 2015; published 20 Jul 2015

the measurements, the waveguides have two bends that provide an offset, d in Fig. 2, of 0.6 mm between the input and output waveguide facets.

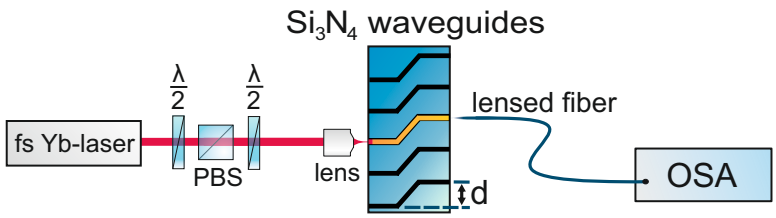

Fig. 2. Experimental setup for on-chip supercontinuum generation. $\lambda/2$: half-wave plate; PBS: polarizing beam splitter; lens: aspheric lens; OSA: optical spectrum analyzer, d: offset between facets to reduce the collection of scattered light.

The supercontinuum spectrum generated in a waveguide with $w = 0.8\ \mu$m, at the maximum available incoupled pulse energy, E_p, of 590 pJ is shown in Fig. 3(a). This pulse energy is limited by the coupling losses. The generated spectrum extends from the blue, at 470 nm at a -30 dB level, and ends in the infrared at 2130 nm. This is, to our knowledge, the widest supercontinuum ever generated on a chip, measured in relative bandwidth (more than 2.1 octaves) as well as absolute bandwidth (more than 495 THz).

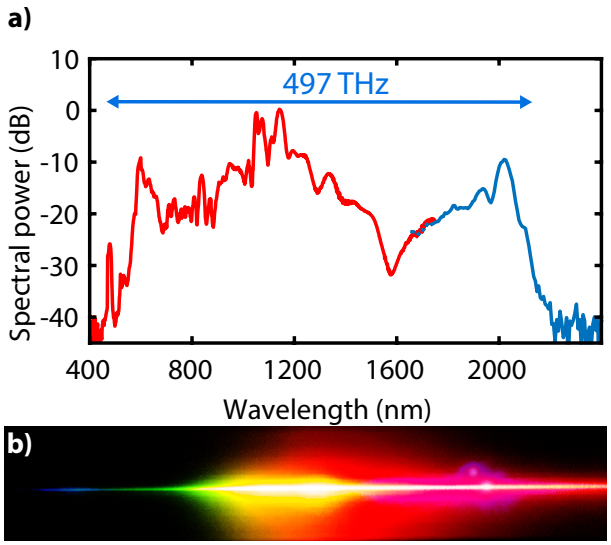

Fig. 3. (a) Supercontinuum spectrum generated in a 5.5 mm long Si_3N_4 waveguide with $h = 1.0\ \mu$m, $w = 0.8\ \mu$m, and $E_p = 590$ pJ. The spectrum extends from 470 nm (at a -30 dB level) to 2130 nm, which is more than 495 THz. The spectrum is measured using an OSA (red) and a near-infrared spectrometer (blue). (b) Photograph of the spectrum after being dispersed by a diffraction grating.

To more systematically characterize the supercontinuum, we measured the output spectra versus incoupled pulse energy of the pump laser. The results for a waveguide with $w = 0.775\ \mu$m are summarized in Fig. 4. One can see that the spectrum continuously broadens with increasing E_p. A dispersive wave becomes noticeable at $E_p = 355$ pJ with its peak at 648 nm. The peak shifts to shorter wavelengths as the power increases, until it reaches 635 nm

#241128 Received 18 May 2015; revised 25 Jun 2015; accepted 26 Jun 2015; published 20 Jul 2015

at $E_p = 462$ pJ. In these experiments, no damaging of the waveguides occurred. However, we found a damage threshold of 1 nJ (incoupled) in other experiments with 10-ps pulses. At low pump energies a small signal can be seen at 532 nm, which we identified to be scattering of infrared pump laser radiation in the OSA. However, this background peak becomes clearly exceeded by visible supercontinuum radiation as the pump energy increases. The blue radiation centered around 480 nm occurs above $E_p = 248$ pJ and is clearly visible in the photograph shown in Fig. 3(b). A small spectral feature centered at 1200 nm can be seen at low pulse energies as well. We found that this background feature consists of weak radiation from the pump laser, but is surpassed by supercontinuum radiation at pump energies beyond 350 pJ.

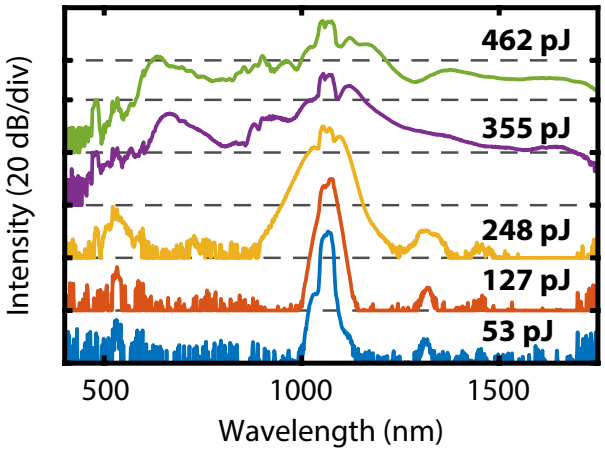

Fig. 4. Spectral broadening of the supercontinuum in a Si_3N_4 waveguide with $w = 0.775$ μm as a function of the incoupled E_p. Note that for visibility a progressive offset of 20 dB was added.

To characterize the supercontinuum as a function of the waveguide dispersion, we injected the pump laser into waveguides of various widths. The results are shown in Fig. 5 for $w = 0.675$ to 0.775 μm. The incoupled E_p differs only slightly from waveguide to waveguide (610 ± 25 pJ) due to some variation in coupling losses. It can be seen that the SCG broadens with increasing w at both the short wavelength side as well as the long wavelength side. This observation is in agreement with what is expected from the broadening of the anomalous dispersion range in Fig. 1(b).

4. Numerical calculations

For a theoretical modeling of the observed SCG, we used the multi-mode nonlinear Schrödinger equation (MM-NLSE, see Appendix) [32]. The equation describes the interaction of multiple transverse modes such as through self and cross-phase modulation, four-wave mixing, and self-steepening. We calculate that for the combination of our spatial pump beam parameters and our waveguide parameters only the fundamental mode (TM_{00}) and one higher order mode (TM_{20}) are excited and that the incoupled pulse energy is estimated to be evenly distributed among the two modes at a wavelength of 1064 nm. The nonlinear coupling coefficient between the fundamental and higher order mode is calculated by evaluating their overlap integral.

In the calculations, we restrict ourselves to the waveguide dimensions that provided the widest SCG as shown in Fig. 3(a) ($h = 1.0$ μm, $w = 0.8$ μm, 5.5 mm propagation length). The effective area of the fundamental mode is calculated to be 0.55 μm^2 for this cross section and the resulting nonlinear coefficient, γ, is 2.6 $W^{-1}m^{-1}$ at a wavelength of 1064 nm. The

#241128 Received 18 May 2015; revised 25 Jun 2015; accepted 26 Jun 2015; published 20 Jul 2015

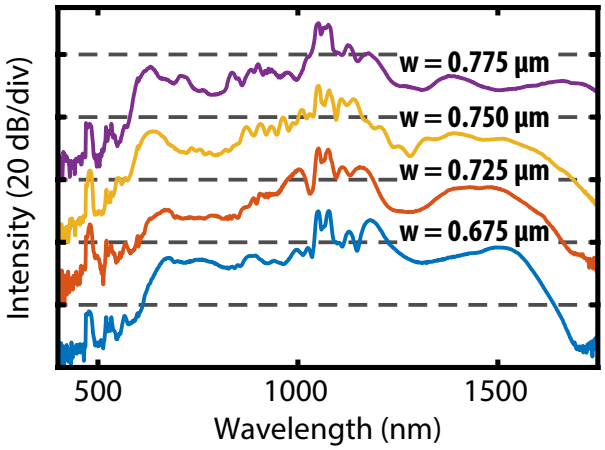

Fig. 5. Supercontinuum generation with various waveguide widths, *w*. The obtained spectrum broadens for wider waveguides. Note that for visibility a progressive offset of 20 dB was added.

corresponding nonlinear length is calculated to be 0.15 mm. In the model the dispersion of the waveguide is included up to the 18th order. The dispersion parameter, *D*, is calculated as 60 ps/(nm km) at the pump wavelength and the resulting dispersion length is 0.37 m. To include a realistic decay of the field amplitudes during propagation we take a propagation loss of 1.3 dB/cm into account, which was measured at the pump wavelength and results in an effective length of 5.1 mm for the waveguide length used. Due to the huge bandwidth of the generated spectrum, it is important to consider the wavelength dependence of the effective mode area and, hence, a wavelength dependence of the nonlinear coefficient. This dependence is introduced by means of a so-called shock term [10]. We neglected the Raman effect, which appears justified in view of previous experiments with SCG in silicon nitride waveguides [19, 21], where Raman scattering did not significantly affect the obtained supercontinuum. As the input light field we take a Fourier-limited pulse with 115 fs duration and a center wavelength of 1064 nm. Calculations show that the chirp introduced by the coupling optics can be neglected.

Figure 6(a) shows the spectrum of the total output (blue) calculated with a total pulse energy of 590 pJ that is equally divided over the fundamental and the higher order mode as in the experiments. In calculations where the pulse energy in the higher order mode was varied we found that the bandwidth of the output spectrum is not sensitive to the amount of pulse energy in the higher order mode, because the mode undergoes normal dispersion in the waveguide. For comparison the measured spectrum from Fig. 3(a) is shown in red. It can be seen that, besides a slight red-shift of the generated spectrum, the overall agreement between the calculated and measured supercontinuum is good. For example, both clearly show the presence of two dispersive waves. A possible reason for the red-shift might be a remaining uncertainty in the refractive index data. Furthermore, we calculated the position of the dispersive waves by their phase-matching condition [33] and found them to lie at 710 nm and 2080 nm, which is in good agreement with the obtained data. Similarly, the generation of blue light at 480 nm, which is observed in the experiments, is not explained with our current model, and a closer investigation is subject of ongoing research. In Fig. 6(b) the spectral broadening during the propagation is shown, calculated such as in Fig. 6(a), and it can be seen that already after a propagation of 2 mm most of the bandwidth is obtained.

#241128 Received 18 May 2015; revised 25 Jun 2015; accepted 26 Jun 2015; published 20 Jul 2015

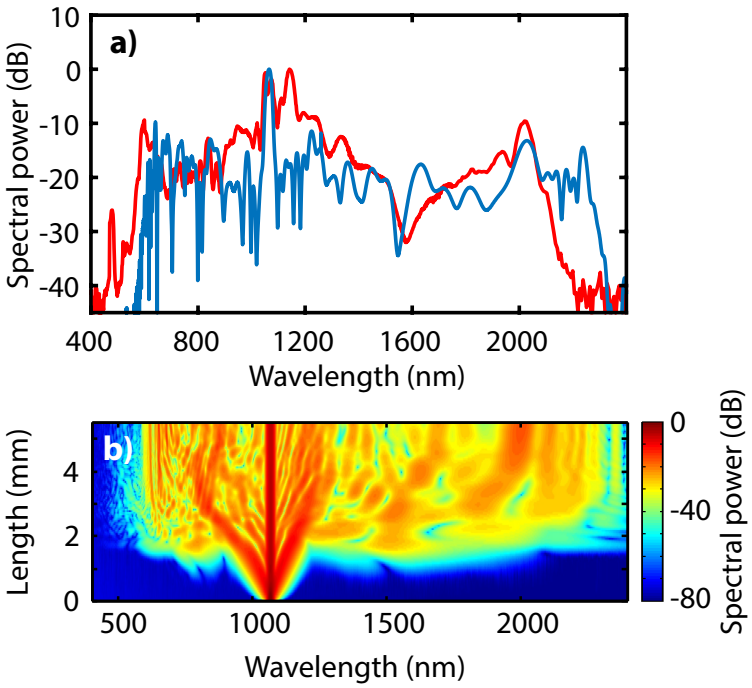

Fig. 6. (a) Comparison of the spectrum modeled with the multi-mode nonlinear Schrödinger equation (blue) and the measured spectrum (red). In the calculation the pulse energy ($E_p = 590$ pJ) and the propagation distance (5.5 mm) are chosen to be the same as in the experiment. (b) Spectral evolution in the numerical calculation as function of propagation distance in the waveguide.

5. Conclusion

In conclusion, we have shown ultra-broadband on-chip supercontinuum generation in CMOS-compatible Si_3N_4 waveguides. When pumped at a center wavelength of 1064 nm with pulses of 115 fs duration, the generated spectrum ranges from the visible blue range (470 nm) to the infrared (2130 nm) and comprises a spectral bandwidth of more than 495 THz. This is, to our knowledge, the widest supercontinuum ever generated on a chip. The measurements show that the bandwidth of the supercontinuum spectrum increases with the incoupled pulse energy and with the waveguide width. A physical model based on the multi-mode nonlinear Schrödinger equation shows that only the fundamental mode contributes to the SCG into which only half of the available pump energy was coupled ($\approx$ 300 pJ). This suggests that a more efficient SCG might be obtained, possibly also with further increased spectral bandwidth. This might be achieved with an improved spatial control of the input coupling, e.g., by means of tapered waveguides, such that all of the available pulse energy is coupled into the fundamental mode.

The wide bandwidths of the spectra demonstrate the huge potential of integrated nonlinear optics using Si_3N_4/SiO_2 waveguides, provided here using the TriPleX platform [30]. The visible to infrared coverage, extending throughout most of the transparency range of Si_3N_4 and SiO_2, appears to be highly attractive for applications such as for self-referencing optical frequency combs [34] on a chip or widely tunable light sources for label-free microscopy and imaging [35] in life sciences.

#241128 Received 18 May 2015; revised 25 Jun 2015; accepted 26 Jun 2015; published 20 Jul 2015

Appendix

The supercontinuum generation in the waveguides presented here was modeled by numerically solving the multimode generalized nonlinear Schrödinger equation (MM-NLSE) which was derived first in reference [32]. We neglect the Raman scattering contribution as it has been reported to not significantly affect SCG in silicon nitride waveguides [19, 21] which yields the following set of equations:

$$\begin{aligned}\frac{\partial A_p}{\partial z} &= i(\beta_p^{(0)} - \beta^{(0)})A_p - \left(\beta_p^{(1)} - \beta^{(1)}\right)\frac{\delta A_p}{\delta t} + i\sum_{n\geq 2}\frac{\beta_p^{(n)}}{n!}\left(i\frac{\delta}{\delta t}\right)^n A_p \\ &+ \frac{in_2\omega_0}{c}\sum_{l,m,n}\left\{\left(1 + i\tau_{plmn}^{(1)}\frac{\partial}{\partial t}\right)\cdot 2Q_{plmn}^{(1)}A_l A_m A_n^* \right. \\ &\left. + \left(1 + i\tau_{plmn}^{(2)}\frac{\partial}{\partial t}\right)\cdot \; Q_{plmn}^{(2)}A_l^* A_m A_n\right\}. \end{aligned} \tag{1}$$

The evolution of the temporal envelope of the mode p, $A_p(z,t)$, is described in a reference frame that travels with the group velocity $\beta^{(1)}$ of the fundamental mode. The electrical field is assumed to have a frequency centered at ω_0 and to travel with a phase velocity of $\beta_p^{(0)} - \beta^{(0)}$, measured relative to the one of the fundamental mode $\beta^{(0)}$. The higher order dispersion coefficients $\beta_p^{(n)}$ are the respective n-th expansion coefficients of the Taylor series of the propagation constant $\beta_p(\omega)$ centered around ω_0, which accounts for the dispersion of the waveguide. The nonlinear interaction of the p-th mode with modes l,m,n is described by the overlap integrals $Q_{plmn}^{(1,2)}$ which can be interpreted as an effective area of the respective nonlinear interaction, $A_{\text{eff},plmn} = 1/(2Q_{plmn}^{(1)} + Q_{plmn}^{(2)})$. The frequency dependence of the nonlinearity is included by the shock-time constants

$$\tau_{plmn}^{(1,2)} = \frac{1}{\omega_0} + \left\{\frac{\delta}{\delta\omega}\ln Q_{plmn}^{(1,2)}(\omega)\right\}_{\omega_0}, \tag{2}$$

taking into account the general dependence of the nonlinearity on the frequency ω as well as a correction to the shock-time by including the change in effective modal area with frequency.

Acknowledgments

This research is supported by the Dutch Technology Foundation STW, which is part of the Netherlands Organisation for Scientific Research (NWO), and which is partly funded by the Ministry of Economic Affairs. We thank W. Hoving (Anteryon BV, The Netherlands) and W. J. Mulder (Avantes BV, The Netherlands) for arranging a short-term loan of the NIR spectrometer.